ACCSCIENCE PUBLISHING

Eurasian Journal of Medicine and Oncology

ORIGINAL RESEARCH ARTICLE

Sulforaphane selectively inhibits glucose metabolism in *PIK3CA*-mutated ovarian cancer cells

Zijiao Li[1†], Yinli Su[2†], Liying Qin[3], Han Wu[1], Wan Fu[1], Xinyu Wang[1], Longyang Li[1], Xuerou Wang[1], Di Chen[4*], Ya Xie[1*], and Linlin Li[3*]

[1]Department of Obstetrics and Gynecology, The First Affiliated Hospital of Zhengzhou University, Zhengzhou, Henan, China

[2]Department of Obstetrics and Gynecology, Fuyang Municipal People's Hospital, Fuyang, Anhui, China

[3]Department of Oncology, The First Affiliated Hospital of Zhengzhou University, Zhengzhou, Henan, China

[4]Department of Pharmacology, School of Pharmaceutical Sciences, Zhengzhou University, Zhengzhou, Henan, China

(This article belongs to the *Special Issue: Tumor Immune Microenvironment and Intervention Strategies*)

[†]*These authors contributed equally to this work.*

***Corresponding authors:**
Linlin Li
(fcclill4@zzu.edu.cn);
Ya Xie
(fccxiey@zzu.edu.cn);
Di Chen
(dichen@zzu.edu.cn)

Citation: Li Z, Su Y, Qin L, *et al.* Sulforaphane selectively inhibits glucose metabolism in *PIK3CA*-mutated ovarian cancer cells. *Eurasian J Med Oncol*. 2026;10(1):245-261.
doi: 10.36922/EJMO025360379

Received: September 4, 2025

Revised: September 25, 2025

Accepted: October 9, 2025

Published online: December 12, 2025

Abstract

Introduction: *PIK3CA* mutations are prevalent in ovarian cancer (OC) and drive cancer progression by activating the phosphatidylinositol 3-kinase (PI3K)/protein kinase B (Akt) pathway. Sulforaphane (SFN), a natural compound derived from cruciferous vegetables, exhibits antitumor effects; however, its specific mechanisms, especially those related to metabolic reprogramming in *PIK3CA*-mutated cancers, remain unclear.
Objective: This study investigates the alterations in glucose metabolism and the selective inhibitory effects of SFN in *PIK3CA*-mutated OC cells.
Methods: Clinical samples from OC patients were analyzed to determine *PIK3CA* mutation status and its prognostic relevance to patient outcome. *PIK3CA*-mutated and wild-type OC cell lines were used for *in vitro* analysis. Glycolysis and mitochondrial respiration were assessed using the Seahorse XF Analyzer. Gene and protein expression were analyzed through RNA sequencing, real-time quantitative polymerase chain reaction, and Western blotting. Metabolite levels were m-easured through untargeted mass spectrometry. The effects of SFN were validated *in vitro* and in a mouse xenograft model.
Results: *PIK3CA* mutations were associated with poorer progression-free survival in OC patients. *PIK3CA*-mutated OC cells exhibited enhanced glycolysis and tricarboxylic acid (TCA) cycle activity compared to wild-type cells. SFN selectively inhibited the proliferation of *PIK3CA*-mutated cells by suppressing glycolysis and the TCA cycle, downregulating key glycolytic enzymes (e.g., hexokinase 1 and 2) and reducing TCA cycle intermediates (e.g., α-ketoglutaric acid and citrate). Mechanistically, SFN inhibited the PI3K/Akt pathway, resulting in reduced Akt phosphorylation. *In vivo*, SFN more effectively inhibited tumor growth in mice bearing *PIK3CA*-mutated xenografts.
Conclusion: *PIK3CA* mutations enhance both glycolysis and the TCA cycle in OC. SFN selectively inhibits the growth of *PIK3CA*-mutated OC cells by targeting the PI3K/Akt pathway, leading to the suppression of glucose metabolism. These findings highlight the therapeutic potential of SFN for *PIK3CA*-mutated OC.

Keywords: *PIK3CA* mutation; Ovarian cancer; Glucose metabolism

1. Introduction

Ovarian cancer (OC) is one of the most common gynecological malignancies worldwide and has the highest mortality rate among them.[1] Although significant progress has been made in treatment strategies, most patients still relapse after treatment and have a poor prognosis.[2] Therefore, new treatments are needed to improve the outcomes of patients with OC.

The transformation of normal cells into cancerous cells involves significant changes in energy metabolism, which is a hallmark of malignancy.[3] Tumor cells tend to produce energy through glycolysis, even when oxygen is sufficient.[4] Enhanced glycolysis supplies both energy and biosynthetic precursors necessary for biological events and acts as an initiator of malignant events in cancer cells.[5] Several well-known oncogenes, including *RAS*,[6] *AMPK*,[7] and *PIK3CA*,[8] play crucial roles in the regulation of metabolic reprogramming to drive cancer progression. Among these, *PIK3CA*, which encodes the catalytic subunit p110α of class I phosphatidylinositol 3-kinases (PI3Ks), is frequently mutated in various cancers, including OC.[9]

PIK3CA mutations, most frequently occurring in exons 9 and 20, particularly at the E545K and H1047R loci, promote tumor growth, invasion, and therapeutic resistance.[10-13] PI3K/protein kinase B (Akt) signaling plays a key role in tumor metabolism, including glycolysis, lipid metabolism, and amino acid metabolism.[14] Prior studies have shown that oncogenic *PIK3CA* mutations can reprogram glutamine metabolism in colorectal cancer. Furthermore, *PIK3CA* mutations may promote metabolic reprogramming by affecting the expression of the hypoxia-inducible factor 1-alpha signaling pathway and genes involved in glycolysis.[15] Targeted treatments of PI3Kα inhibitors, such as alpelisib and GDC-0941, have been developed to target *PIK3CA* mutations.[16-18] However, drug resistance and adverse effects limit their efficacy,[19] necessitating the search for safer and more effective treatments.

Sulforaphane (SFN), a naturally occurring compound found in cruciferous vegetables, exerts anti-inflammatory, antioxidant, and anticancer effects by modulating key cellular pathways.[20-22] SFN enhances the efficacy of chemotherapy and reverses drug resistance.[23-27] Prior studies have shown that SFN inhibits glycolysis and cell proliferation by targeting the TBX15/KIF2C pathway in gastric cancer cells;[28] however, the specific mechanisms by which SFN affects tumor metabolism in *PIK3CA*-mutated cancers remain unclear.

Therefore, in this study, we explore the alterations in glucose metabolism in *PIK3CA*-mutated OC cells and further elucidate the selective inhibitory effects and underlying mechanisms of SFN. Moreover, we evaluate the effect of SFN on OC progression through *in vivo* experiments to assess its therapeutic potential for clinical application.

2. Methods

2.1. Patient tissue samples

In this study, all OC patients were recruited from the First Affiliated Hospital of Zhengzhou University, where they were diagnosed through histopathological examination (Table S1). We assessed the association between *PIK3CA* mutation status and progression-free survival (PFS). The samples were collected between January 2007 and October 2024. The study was approved by the Ethics Committee of the First Affiliated Hospital of Zhengzhou University. In addition, all experiments were conducted in accordance with relevant guidelines and regulations. Informed consent was obtained from all participants and/or their legal guardians. All research involving human participants was conducted in accordance with the Declaration of Helsinki. The patient selection process is illustrated in Figure S1, and the inclusion and exclusion criteria are provided in Table S2.

2.2. Reagents and antibodies

SFN (>98%) powder (S111997) was purchased from Shanghai Aladdin Biochemical Technology (China). A 100 mM stock solution of SFN was prepared in dimethyl sulfoxide (DMSO; Meilunbio, China) and stored at −20°C until further use. The final concentration of DMSO in each treatment group did not exceed 0.1%. SC79 ($C_{17}H_{17}ClN_2O_5$; HY-18749) was purchased from MedChemExpress (USA). The cell culture medium, fetal bovine serum (FBS), and phosphate-buffered saline (PBS) were obtained from Biological Industries (Israel). The primary antibodies against hexokinase 1 (HK1; BF0126; 1:2000), pyruvate dehydrogenase kinase 2 (PDK2; DF4366; 1:1000), glucose transporter 1 (GLUT1; AF0173; 1:1000), and pyruvate kinase 2 (PKM2; AF5234; 1:1000) were purchased from Affinity Biosciences (USA). The primary antibodies against hexokinase 2 (HK2; 2867T; 1:1000), lactate dehydrogenase A (LDHA; 3582T; 1:1000), serine/threonine kinase (AKT; 4691T; 1:2000), and phosphorylated AKT (Phospho-AKT [Ser473]; 4060T; 1:2000) were purchased from Cell Signaling Technology (USA). Citrate synthase (CS; 16131-1-AP; 1:2000), isocitrate dehydrogenase1 (IDH1; 12332-1-AP; 1:3000), IDH2 (15932-1-AP; 1:2000), and oxoglutarate dehydrogenase (OGDH; 15212-1-AP; 1:1000) were purchased from Proteintech (USA). The primary antibody 6-phosphofructo-2-kinase/fructose-2,6-bisphosphatase 3 (PFKFB3; ab181861; 1:4000) and β-actin (ab8827;

1:1000) were purchased from Abcam (United Kingdom). The enhanced chemiluminescence kit, thiazolyl blue tetrazolium bromide (MTT), and Cell Counting Kit-8 were purchased from Meilunbio (China).

2.3. Animal studies

All animal experiments were approved by the Animal Care Committee of the First Affiliated Hospital of Zhengzhou University. In addition, all experiments were conducted in accordance with relevant guidelines and regulations. The studies involving live animals were conducted in accordance with the Animal Research: Reporting of *In Vivo* Experiments guidelines. Female BALB/c mice ($n = 16$; SPF (Beijing) Biotechnology Co., Ltd, China) were maintained in a specific pathogen-free environment. To investigate the effect of SFN on OC, we divided the animals into four groups: (i) Mutant OC (OVCAR3-M) + PBS, (ii) OVCAR3-wild-type (WT) + PBS, (iii) OVCAR3-M + SFN, and (iv) OVCAR3-WT + SFN, with four animals in each group. Mice in the SFN group received an oral dose of 25 mg/kg/day of SFN. Control mice received an equal amount of PBS. The body weight of the mice was recorded every 3 days. Treatment continued for 28 days in the SFN-administered groups. Animal anesthesia and animal euthanasia were performed in accordance with the American Veterinary Medical Association guidelines for animal euthanasia. Briefly, ketamine (100 mg/kg) and xylazine (10 mg/kg) were injected into the abdominal cavity. After confirming the absence of the paw withdrawal reflex, euthanasia was performed via cervical dislocation. Death was verified by the absence of pulse and respiration, along with fixed, dilated pupils persisting for more than 5 min. No animal regained consciousness before tissue collection.

2.4. Cell lines

The A2780 and OVCAR3 cell lines were purchased from the Cell Bank of the Chinese Academy of Sciences (China). Cells were maintained at 37°C in RPMI-1640 medium supplemented with 10% FBS and 1% penicillin/streptomycin (streptomycin 100 μg/mL, penicillin 100 U/mL) in a humidified incubator with 5% carbon dioxide.

2.5. Cellular glycolytic stress experiment

The appropriate amount of cell suspension was evenly seeded onto a Seahorse XF96 cell culture plate (Agilent, USA) and incubated under standard conditions. After cell attachment, the culture medium was replaced with medium containing different concentrations of SFN (0 and 20 μM). Each well received 80 μL of the respective treatment medium and was incubated for 24 h. Following treatment, the medium was aspirated using a pipette on an ultra-clean bench, and the cells were washed 3 times with pre-warmed assay medium containing 1 mM glutamine XF base medium at 37℃. After adding 80 μL of pre-warmed assay solution to each well, the plates were incubated at 37°C in a non-carbon dioxide incubator for 45–60 min to induce glucose starvation. The hydrated sensor cartridge (prepared 1 day prior) was then loaded with glucose, oligomycin, and 2-deoxyglucose into ports A, B, and C, respectively, according to the manufacturer's protocol. The glycolytic stress test was performed using the Seahorse XF96 Analyzer (Agilent, USA) following calibration of the sensor plate. Data were collected and analyzed using the Seahorse Bioscience Wave software (version Wave 2.5.0; Agilent, USA). All experiments were conducted in triplicate using independent biological replicates.

2.6. Cell mitochondrial stress test

A cell suspension with moderate density was evenly seeded onto Seahorse XF96 cell culture plates and allowed to settle for 2 h before incubation. After cell attachment, the culture medium was aspirated under aseptic conditions and replaced with medium containing different concentrations of SFN (0 and 20 μM). Each well received 80 μL of the corresponding treatment medium and was incubated at 37℃ in a 5% carbon dioxide incubator. After treatment, the cells were washed 3 times with pre-warmed XF base medium (37℃) containing 1 mM pyruvate, 2 mM glutamine, and 10 mM glucose. Subsequently, 80 μL of pre-warmed assay solution was added to each well. Following the manufacturer's protocol, oligomycin, the mitochondrial uncoupler FCCP, and the electron transport chain inhibitors rotenone and antimycin A were sequentially loaded into injection ports A, B, and C, respectively. The mitochondrial stress test was then conducted using the Seahorse XF96 Analyzer, and data were analyzed using the Wave software. All experiments were performed in triplicate using independent biological replicates.

2.7. RNA sequencing

Stable OC cell lines were seeded in 6-well plates and treated with varying doses of SFN (0 or 30 μM) for 24 h. Total RNA was extracted using TRIzol (Invitrogen, USA). RNA quality and concentration were determined using a microplate spectrophotometer (Thermo Scientific NanoDrop One/OneC Microvolume UV-Vis Spectrophotometer, Thermo Scientific, USA). Samples were transported on dry ice to Berry Genomics (China) for transcriptome sequencing and bioinformatics analysis. Data were derived from three independent biological replicates.

2.8. Untargeted mass spectrometry detection

The OVCAR3-WT and OVCAR3-M cells, in the logarithmic growth phase, were divided into experimental and control groups. After 24 h of incubation, the control group was replaced with freshly prepared drug-free medium (with the same concentration of DMSO as the dissolved drug), whereas the experimental group was replaced with medium containing the drug at its respective half-maximal inhibitory concentration for each cell line. The cells were then incubated for an additional 24 h. After washing with PBS, the cells in the experimental group were frozen at −80°C for 30 min. Following another PBS wash, 1.5 mL of methanol–water solution (4:1, v/v) was added to each dish, and the cells were again frozen at −80°C for 30 min. The cells were then collected into centrifuge tubes using a cell scraper. An additional 1.5 mL of pre-cooled methanol–water (4:1, v/v) was added to each dish to fully recover any residual cells. All procedures were performed on ice. Subsequently, 1 mL of chloroform was added to each sample, and the cells were disrupted using an ultrasonic homogenizer. After centrifugation, both the upper and lower layers were carefully transferred into new centrifuge tubes, mixed thoroughly, and concentrated to dryness using a vacuum concentrator. To each dried sample, 100 μL of methanol solution containing a mixed isotope internal standard was added for the experimental group. For the control group, a proportional volume of the same methanol solution was added based on the cell count ratio relative to the experimental group. Samples were sonicated to ensure complete dissolution, centrifuged, and the resulting supernatants were filtered through a 0.22 μm organic membrane before analysis. Data were derived from three independent biological replicates.

2.9. Western blotting

Cells were treated with different drugs and/or media for the indicated durations, washed 3 times with PBS, and lysed on ice for 30 min using a radio-immunoprecipitation assay lysis buffer supplemented with 1 mM phenylmethylsulfonyl fluoride and 10 mM phosphatase inhibitors. The lysates were centrifuged at 4°C to remove cellular debris, and the supernatants containing total protein were collected. Protein concentrations were determined using a bicinchoninic acid protein assay kit (Beyotime Biotech Inc., China) according to the manufacturer's instructions. Equal amounts of protein were separated by sodium dodecyl sulfate-polyacrylamide gel electrophoresis and transferred onto nitrocellulose membranes at 100 V for 90 min. The blots were incubated for 2 h with a Tris-buffered saline buffer containing 5% skimmed milk powder, followed by an overnight incubation with primary antibodies diluted in the buffer solution at 4°C. This was followed by incubation with relevant secondary antibodies for 2 h at room temperature. Protein bands were visualized using the enhanced chemiluminescence assay kit (Meilunbio, China). Protein expression levels were quantitatively determined using ImageJ (version 1.53k; National Institutes of Health, USA). β-actin was used as an internal reference for protein expression. Original images of the Western blots are provided in Figures S4-S11. Data were derived from three independent biological replicates.

2.10. RNA extraction and quantitative real-time polymerase chain reaction

Total RNA was extracted from the cells using TRIzol and then reverse-transcribed into cDNA using a cDNA reverse transcription kit (Takara, China). The primer sequences used for the real-time quantitative polymerase chain reaction (RT-qPCR) are displayed in Table S3. The QuantStudio 5 Real-time PCR system (Thermo Scientific, USA) was used for RT-qPCR analysis.

2.11. Cell proliferation assay

The proliferation capacity of OC cells was assessed using the Cell Counting Kit-8 assay. Cells were seeded into 96-well plates (2×10^4/well), and at the indicated time-points, the old medium was replaced with 100 μL of fresh medium containing 10 μL of Cell Counting Kit-8 solution. After 4 h of incubation at 37°C, the absorbance levels for each sample at 450 nm were measured using a Multiskan Ascent Plate reader (Thermo Electron, USA). Data were derived from three independent biological replicates.

2.12. Cell viability assay

The effects of SFN or MK2206 (MedChemExpress, China) on cell viability were detected using an MTT assay. Cells were seeded into 96-well plates (6×10^4/well) and treated with various concentrations of SFN (0, 1.25, 2.5, 5, 10, 20, 40, and 80 μM). At the indicated time-points, the old medium was replaced with 100 μL of fresh medium containing 20 μL of MTT solution (5 mg/mL in PBS). After 4 h of incubation at 37°C, formazan crystals were completely solubilized with 150 μL DMSO in each well. The absorbance levels for each sample at 540 nm were measured. All experiments were independently repeated at least 3 times.

2.13. Overexpression of lentivirus transfection

According to the full-length cDNA sequence of the human *PIK3CA* gene in GenBank, *PIK3CA*-E545K mutant and WT viral vectors were constructed using CMV-MCS-3flag-polyA-EF1A-zsGreen-sv 40-puromycin as the skeleton. Virus packaging was performed by Shanghai Jikai Gene (China).

2.14. Statistical analyses

GraphPad Prism 8.0.1 was used for statistical analysis and statistical graphing. Continuous variables are presented as mean ± standard deviation. The *t*-test or paired *t*-test was used to compare differences between two groups, whereas the analysis of variance or repeated-measures analysis of variance was used to test the differences in means between multiple groups. The Kaplan–Meier method was used for survival analysis, and the log-rank test was used to compare differences between groups. All statistical tests were two-sided, and a $p < 0.05$ was considered statistically significant.

3. Results

3.1. High prevalence of *PIK3CA* variants correlates with poor prognosis in OC

To characterize the genetic alterations in OC, we collected samples from 128 patients at the Affiliated Hospital of Zhengzhou University for next-generation sequencing analysis. As shown in Figure 1A and B, among the 128 cases, the top 10 mutated genes were *TP53*, *BRCA1/2, NF1*, *ARID1A*, *KRAS*, *PIK3CA*, *APC*, *FAT1*, *ARID1B*, and *CREBBP*. *PIK3CA* ranked sixth (12/128, 9.4%), whereas *TP53* was the most frequently mutated gene (106/128, 82.8%). *PIK3CA* mutations were observed in 12 patients, with the most common mutation being p.H1047R (c.3140A>G) in exon 20, accounting for 50% (6/12) of the cases. This was followed by mutations in exon 9 (33.3%), including one case of p.Q546K, one case of p.E545K, one case of p.E546K, and one case of p.E545G. *PIK3CA* copy number amplifications were observed in five cases (3.9%), fewer than the number of mutation cases. Since both *PIK3CA* mutations and copy number variations are considered gain-of-function alterations, they were included in subsequent data analyses.

We further examined the co-occurrence of *PIK3CA* mutations with other genetic alterations. Among the 17 cases with *PIK3CA* mutations, 11 (64.7%) also harbored *TP53* mutations. In addition, 6 cases (35.3%) had *BRCA1/2* mutations, and 5 (29.4%) had *ARID1A* mutations. Although *NF1* and *KRAS* mutations are common in OC, they did not co-occur with *PIK3CA* mutations. Thus, *PIK3CA* mutations frequently co-existed with *TP53*, *BRCA1/2*, and *ARID1A* mutations, and were mutually exclusive with *NF1* and *KRAS* (Figure 1C).

We then analyzed the association between *PIK3CA* variants and various clinicopathological characteristics using a multivariable logistic regression model (Figure 1D). *PIK3CA* mutations were not associated with age, tumor stage, the International Federation of Gynecology and Obstetrics grade, estrogen receptor/progesterone receptor status, or Ki-67 index. To evaluate the prognostic impact of *PIK3CA* mutations in OC, we compared PFS (the time from first-line surgery combined with chemoradiotherapy to the first disease progression) between the *PIK3CA* mutation group and the WT group. Kaplan–Meier analysis revealed that the PFS was significantly shorter in the *PIK3CA* mutation group compared to the WT group (95% confidence interval: 21.51–36.49, p=0.042) (Figure 1E). Collectively, these findings suggest that *PIK3CA* mutations are associated with poor prognosis in OC.

3.2. *PIK3CA*-mutated cells exhibit higher levels of glycolysis in OC

To assess the impact of *PIK3CA* mutations on cellular glucose metabolism, we verified the expression of *PIK3CA* in *PIK3CA*-mutated A2780 cells and in OVCAR3 cells with WT *PIK3CA* (Figure 2A). We employed the Seahorse XF96 Analyzer to monitor real-time cellular metabolic activity. As shown in Figure 2B, the glycolytic rate, glycolytic capacity, and glycolytic reserve were significantly increased in *PIK3CA*-mutated A2780 cells compared to *PIK3CA* WT OVCAR3 cells. Subsequently, OVCAR3 cells were transduced with *PIK3CA*-wild and *PIK3CA*-E545K viruses to generate stable OC cell lines overexpressing either WT or mutant *PIK3CA* (OVCAR3-WT and OVCAR3-M, respectively) (Figure 2C). Similarly, glycolytic levels were elevated in OVCAR3-M cells compared to OVCAR3-WT cells (Figure 2D). The upregulation of glycolysis supports the production of biosynthetic precursors necessary for cell proliferation. As demonstrated by cell growth assays, *PIK3CA*-mutated cells (A2780 or OVCAR3-M) exhibited a higher proliferation rate than *PIK3CA* WT cells (OVCAR3 or OVCAR3-WT) in a time-dependent manner (Figure 2E and F). These findings indicate that *PIK3CA* mutations enhance glycolysis in OC cells, thereby promoting their proliferation.

To investigate the mechanism by which *PIK3CA* mutations enhance glycolysis, we extracted mRNA from *PIK3CA*-mutated and WT cells (OVCAR3-M vs. OVCAR3-WT) and performed transcriptome sequencing to analyze gene expression differences (Figure 2G). The results revealed that, compared to the control group, the expression of the glucose transporter (*SLC2A1*, encoding GLUT1) and glycolysis-related enzymes was significantly upregulated, including HK1, HK2, PKM2, LDHA, glyceraldehyde-3-phosphate dehydrogenase, pyruvate dehydrogenase 1, and PFKFB3 (Figure 2H and I). Furthermore, we also verified the sequencing results using RT-qPCR, and the results were consistent with those obtained by sequencing (Figure S2). In addition, Western blot analysis confirmed that the protein levels of HK1 and

A

Gene	Mutation cases *n* (%)	CNV cases *n* (%)	Total *n* (%)
TP53	106 (82.8%)	0 (0.0%)	106 (82.8%)
BRCA1/2	65 (50.8%)	0 (0.0%)	65 (50.8%)
NF1	17 (13.3%)	2 (1.6%)	19 (14.8%)
ARID1A	16 (12.5%)	0 (0.0%)	16 (12.5%)
KRAS	15 (11.7%)	2 (1.6%)	17 (13.3%)
PIK3CA	13 (10.2%)	4 (3.2%)	17 (13.3%)
APC	12 (9.4%)	0 (0.0%)	12 (9.4%)
FAT1	12 (9.4%)	0 (0.0%)	12 (9.4%)
ARID1B	10 (7.8%)	0 (0.0%)	10 (7.8%)
CREBBP	10 (7.8%)	0 (0.0%)	10 (7.8%)

B

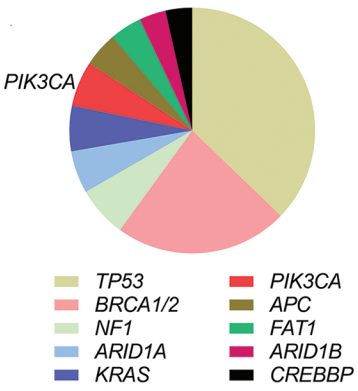

C

Clinical pathological features	*PIK3CA* status	Wild type(*n*)	Mutant(*n*)
KRAS	wild	97	14
	mut	14	3
BRCA	wild	49	11
	mut	62	6
PTEN	wild	95	16
	mut	3	1
TP53	wild	11	6
	mut	100	11
ARID1A	wild	99	12
	mut	12	5

D

Clinical pathological characteristics	*PIK3CA* status Wild type (*n*)	Mutant (*n*)	χ^2	*p*
Total cases (*n*)	111	17		
Age (years)				
≤50	38	6	0. 007	0. 932
>50	73	11		
Pathological type				
Serous	96	11	3. 735	0. 357
Other	15	6		
FIGO stage				
I-II	9	3	0. 656	0. 418
III-IV	102	14		
ER				
Negative	30	8	2. 834	0. 092
Positive	81	9		
PR				
Negative	56	10	0. 414	0. 520
Positive	55	7		
Ki67				
Weak positive	17	2		
Positive	23	4	0. 188	0. 910
Strong positive	71	11		

E

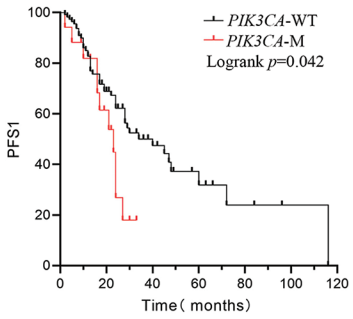

Figure 1. Clinical data analysis of 128 ovarian cancer (OC) patients. (A and B) The top 10 most common gene mutations in OC patients. (C) The relationship between clinical pathological characteristics and *PIK3CA* status. (D) The association between *PIK3CA* mutations and clinical pathological characteristics in OC patients. (E) Analysis of the correlation between *PIK3CA* mutation status and progression-free survival (PFS) after first-line treatment in OC patients. Survival curves were compared using the log-rank test; the *p*-values are indicated. Statistical significance determined at **p*<0.05; ***p*<0.01; ****p*<0.001; and *****p*<0.0001.

Abbreviations: ER: Estrogen receptor; M: Mutant; PR: Progesterone receptor; WT: Wild-type.

HK2 were upregulated in *PIK3CA*-mutated cells (A2780 or OVCAR3-M) compared to WT cells (OVCAR3 or OVCAR-WT), whereas no significant differences were observed in the protein levels of GLUT1, PFKFB3, and LDHA (Figure 2J and K).

The PI3K/Akt pathway is an important regulator of glycolysis-related enzymes, and mutations in *PIK3CA* can lead to sustained PI3K/Akt activation. Therefore, we evaluated the expression and phosphorylation status of proteins in the PI3K/Akt pathway in OC cells. As shown in Figure 2L, the expression of p-AKT (ser473) protein increased significantly in *PIK3CA*-mutated cells, with no difference in PI3K and AKT total protein expression. This suggests that mutant OC cells may upregulate the

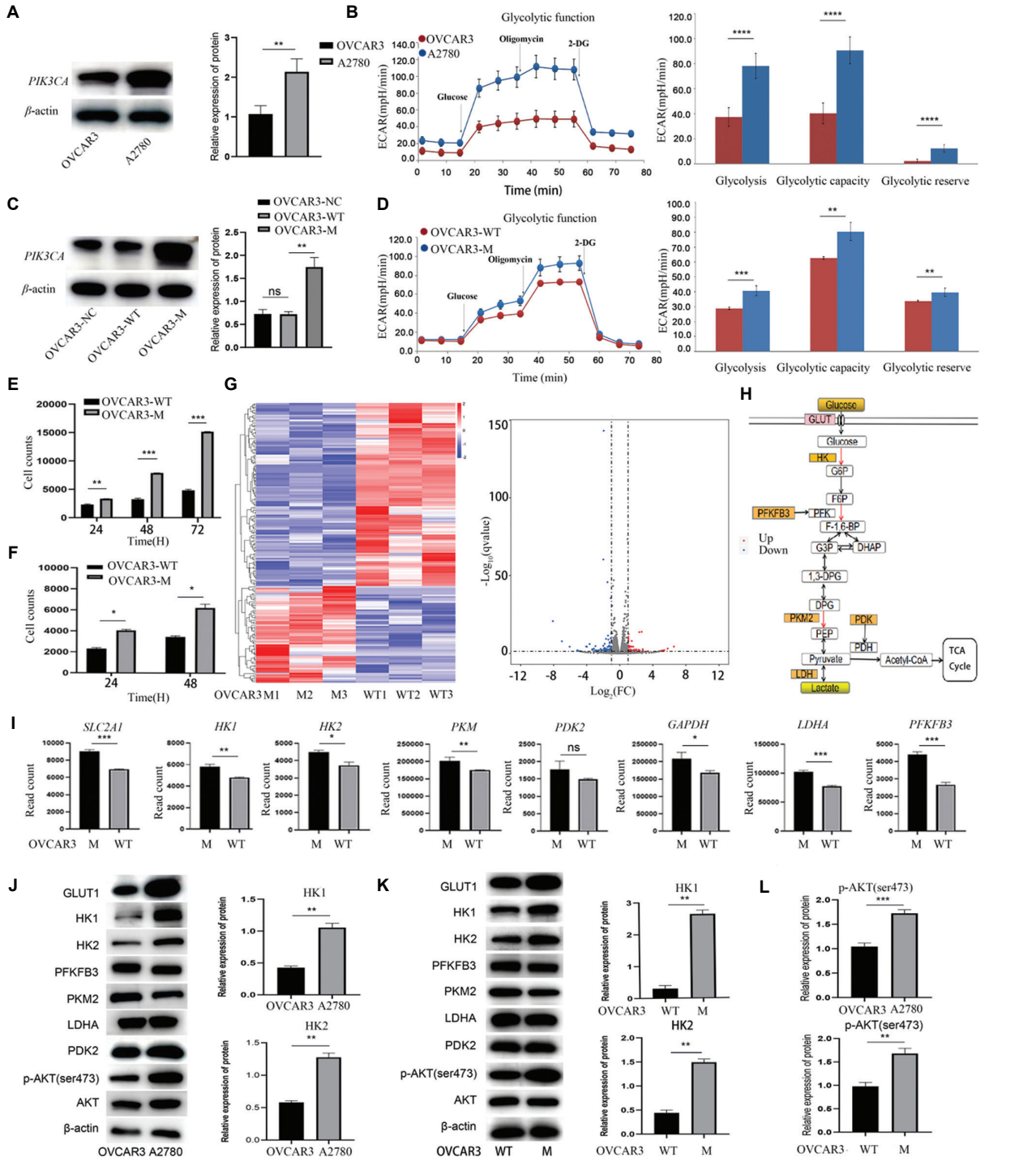

Figure 2. *PIK3CA*-mutated cells exhibit higher levels of glycolysis and tricarboxylic acid (TCA) cycle activity in ovarian cancer (OC). (A) Western blot analysis of phosphatidylinositol 3-kinase (PIK3CA) protein expression in A2780 and OVCAR3 cells. (B) Glycolysis stress test performed on A2780 and OVCAR3 cells. (C) Western blots of PIK3CA protein expression in negative control OVCAR3, OVCAR3-WT (wild type), and OVCAR3-M (mutant) cells. (D) Glycolysis stress test performed on OVCAR3-WT and OVCAR3-M cells. (E and F) Differences in proliferation capacity over time between A2780 and OVCAR3, OVCAR3-WT, and OVCAR3-M cells. (G) Heatmap of gene sequencing and volcano plot showing differential gene expression between OVCAR3-M and OVCAR3-WT. (H) Schematic diagram of the glycolytic pathway and the pyruvate metabolism destination. (I) Differential expression of glycolysis-related genes from gene sequencing data. (J & K) Protein-level detection showing differences in glycolysis-related enzymes between A2780 and OVCAR3, OVCAR3-WT, and OVCAR3-M cells. (L) The *PIK3CA* mutation activates the downstream protein kinase B (AKT). Data from three independent experiments are shown as mean ± standard deviation. Statistical significance determined at *p<0.05; **p<0.01; ***p<0.001; and ****p<0.0001; ns indicates not significant.
Abbreviations: ECAR: Extracellular acidification rate; FC: Fold change; HK: Hexokinase.

expression of HK1 and HK2 by activating the PI3K/Akt signaling pathway.

3.3. *PIK3CA*-mutated cells exhibit higher levels of tricarboxylic acid (TCA) in OC

Energy metabolism analysis revealed that basal oxygen consumption, reserve respiratory capacity, and oxygen consumption related to adenosine triphosphate production were significantly increased in *PIK3CA*-mutated cells (A2780 or OVCAR3-M) compared to *PIK3CA* WT cells (OVCAR3 or OVCAR3-WT), as shown in Figure 3A and B. The enhanced oxygen consumption rate in mutant cells indicates an increase in aerobic oxidation, specifically in the TCA cycle. To investigate the mechanism by which *PIK3CA* mutations enhance aerobic oxidation, especially in the TCA cycle, we extracted mRNA from OVCAR3-WT and OVCAR3-M cells and performed transcriptome sequencing to analyze differences in gene expression. The results showed that the TCA key enzymes in OVCAR3-M exhibited no significant change compared to those in OVCAR3-WT (Figure 3C). In addition, we found no significant changes in the relevant enzymes of the TCA cycle using Western blot analysis (Figure 3D). This suggests that the enhancement of the TCA cycle in *PIK3CA*-mutated cells may not be due to the increased activity of key enzymes in the TCA cycle.

The carbon sources for the TCA cycle can be replenished by glutamine. To investigate whether *PIK3CA* mutations affect the replenishment of the TCA cycle with glutamine in OC cells, we conducted an untargeted metabolomics analysis to detect small-molecule metabolites in mutant and WT OVCAR3 cells. As shown in Figure 3E, compared to WT cells, mutant cells exhibited increased levels of α-ketoglutaric acid (α-KG), citrate, and succinic acid in the TCA cycle, whereas glutamine levels were decreased. Moreover, we detected a significant increase in glutathione, one of the key products synthesized from glutamine, which may be due to the increased demand for antioxidant capacity caused by the *PIK3CA* mutations.

To clarify whether the more robust TCA cycle (Figure 3F) in mutant cells is driven by enhanced glutamine replenishment, we performed Western blot analysis of glutamine-related enzyme expression in both mutant and WT cells. As shown in Figure 3G, the results indicated no significant differences in the protein expression levels of key enzymes in the glutamine pathway and the TCA cycle, such as glutaminase, glutamate oxaloacetate transaminase 1, glutamate oxaloacetate transaminase 2, glutamic-pyruvic transaminase, and glutamate dehydrogenase between mutant and WT cells. The findings suggest that, because glutamine depletion was not associated with increased α-KG production, metabolic flux analysis indicated that decreased glutamine levels were accompanied by elevated glutathione levels, suggesting diversion of glutamine toward glutathione synthesis. This indicates that glutamine may be redirected toward glutathione synthesis. Therefore, the enhanced TCA cycle activity in mutant cells is likely due to increased glycolysis.

3.4. SFN selectively inhibits glycolysis in *PIK3CA*-mutated cells

To evaluate the inhibitory effect of SFN on different cell lines, we assessed SFN cytotoxicity in two cell types using the MTT assay and calculated the half-maximal inhibitory concentration of SFN in each cell line. The results demonstrated that SFN more effectively inhibited the proliferation of *PIK3CA*-mutated cells compared to the WT cells (Figure 4A and B). Based on previous findings showing higher expression of glycolysis-related enzymes in mutant cells, we hypothesized that SFN might target the enhanced glycolytic activity in *PIK3CA*-mutated cells, leading to the observed differential inhibitory effects.

To investigate this, we measured the extracellular acidification rate in the OC cells following SFN treatment for 24 h. Remarkably, SFN significantly suppressed the extracellular acidification rate in OC cells, with a more pronounced inhibition of glycolytic rate, glycolytic capacity, and glycolytic reserve in *PIK3CA*-mutated cells compared to WT cells (Figure 4C). We further validated these results in transfected cell lines, which confirmed consistency with our initial findings (Figure 4D).

SFN treatment also downregulated glycolysis-related enzymes, particularly in *PIK3CA*-mutated OC cells. To confirm whether the inhibitory effects of SFN on mutant cells were mediated through the suppression of glycolysis-related enzymes, we conducted Western blot analysis across the OC cell lines. The results showed that SFN inhibited the expression of HK1, HK2, GLUT1, PKM2, and PFKFB3 in OC cells, with a stronger inhibitory effect in mutant cells compared to WT cells (Figure 4E). Similar results were obtained in stable cell lines, reinforcing our previous observations (Figure 4F). These findings suggest that SFN reduces the expression of glycolysis-related enzymes in OC cells, with a particularly strong effect in *PIK3CA*-mutated cells. Based on these results, we speculate that SFN exerts a stronger anti-proliferative effect on *PIK3CA*-mutated cancer cells by inhibiting their glycolytic activity.

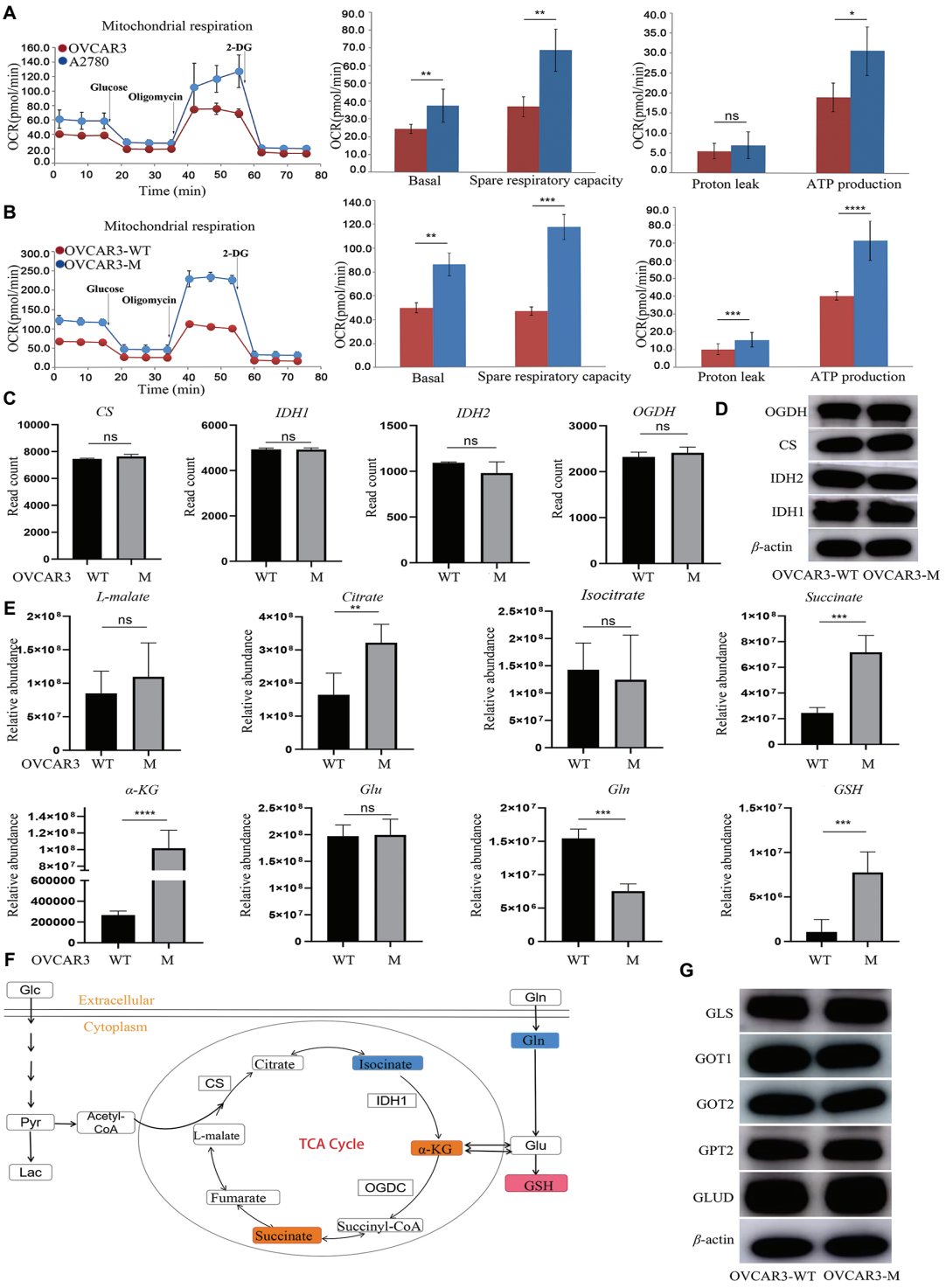

Figure 3. *PIK3CA*-mutated cells exhibit higher levels of aerobic oxidation in ovarian cancer (OC). (A and B) Mitochondrial stress test performed on A2780, OVCAR3, OVCAR3-WT (wild-type), and OVCAR3-M cells (mutant). (C) Differential expression of tricarboxylic acid (TCA) cycle-related genes from gene sequencing data. (D) Protein-level detection of key enzymes involved in the TCA cycle in OVCAR3-WT and OVCAR3-M cells. (E) Metabolite analysis of A2780 and OVCAR3 cells. (F) Schematic of the TCA cycle. (G) Protein-level detection of key enzymes involved in the glutamine cycle in OVCAR3 and A2780 cells. Data from three independent experiments are shown as mean ± standard deviation. Statistical significance determined at *p<0.05; **p<0.01; ***p<0.001; and ****p<0.0001; ns indicates not significant.

Abbreviations: α-KG: Alpha-ketoglutarate; ATP: Adenosine triphosphate; Gln/GLS: Glutaminase; Glu: Glutamine; GLUD: Glutamate dehydrogenase; GOT: Glutamic-oxaloacetic transaminase; GPT: Glutamic-pyruvate transaminase; GSH: Glutathione; OCR: Oxygen consumption rate.

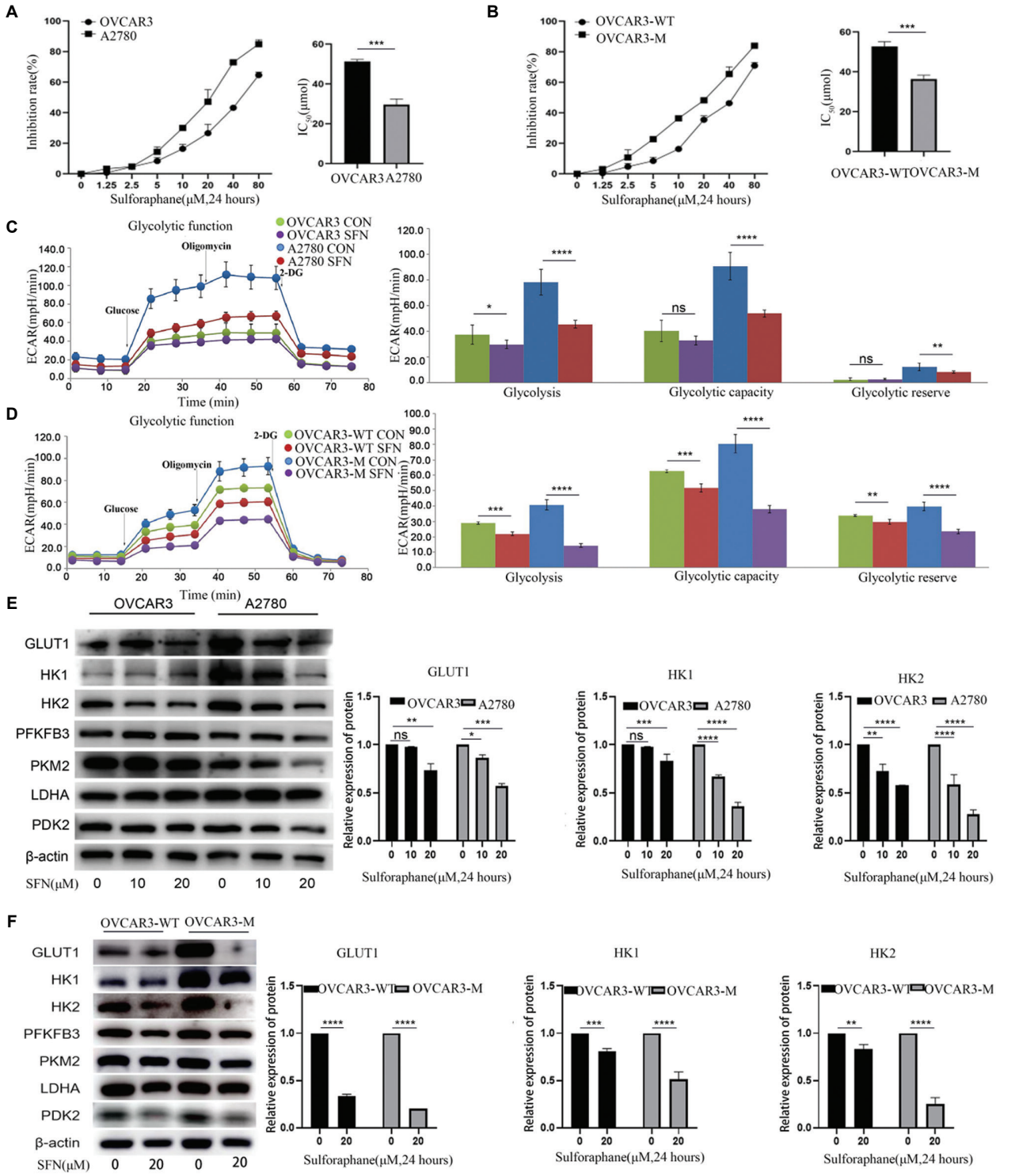

Figure 4. Sulforaphane (SFN) selectively inhibits glycolysis in *PIK3CA*-mutated cells. (A and B) CCK-8 assay showing the inhibitory rate of four ovarian cancer (OC) cell lines after 24 h of treatment with different concentrations of SFN. (C and D) Glycolysis stress test performed on A2780 and OVCAR3 cells after 24 h of treatment with or without 20 μM SFN, and on OVCAR3-WT (wild-type) and OVCAR3-M (mutant) cells after similar treatment. (E) Changes in the expression of glycolysis-related enzymes in A2780 and OVCAR3 cells after treatment with different concentrations of SFN (0, 10, 20 μM). (F) Changes in the expression of glycolysis-related enzymes in OVCAR3-WT and OVCAR3-M cells after treatment with or without 20 μM SFN. Data from three independent experiments are shown as mean ± standard deviation. Statistical significance determined at *$p<0.05$; **$p<0.01$; ***$p<0.001$; and ****$p<0.0001$; ns indicates not significant.

Abbreviations: ECAR: Extracellular acidification rate; GLUT1: Glucose transporter 1; HK: Hexokinase.

3.5. SFN selectively inhibits glycolysis in *PIK3CA*-mutated cells through phosphoinositide 3-kinase/protein kinase B/hexokinase signaling

Next, we examined whether SFN regulates key enzymes in the glycolysis pathway by modulating the PI3K/Akt signaling pathway. To this end, we analyzed p-AKT protein expression in transfected cells pretreated with SFN. The results indicated that SFN effectively inhibited p-AKT protein expression, with a more pronounced effect in *PIK3CA*-mutated cells compared to WT cells, whereas total AKT levels remained unchanged in both groups (Figure 5A). This suggests that the *PIK3CA* mutation activates downstream Akt signaling, which subsequently regulates glycolysis-related enzymes to promote the proliferation of cancer cells. SFN, by reducing the expression of key glycolytic enzymes, inhibits cancer cell proliferation and selectively suppresses the growth of tumor cells.

To further validate this hypothesis, we treated OVCAR3-WT and OVCAR3-M cells with MK2206, an AKT inhibitor (Figure 5B). Western blot analysis revealed that treatment with the AKT inhibitor reduced cell proliferation and decreased the expression of key glycolytic enzymes, including HK1, HK2, and GLUT1. These findings were consistent with the effects observed following SFN treatment (Figure 5C and D). These results support the notion that *PIK3CA* mutations activate the PI3K/Akt pathway, thereby enhancing glycolysis and promoting cancer cell proliferation. In addition, to further verify that SFN inhibits glycolysis by inhibiting the PI3K/Akt pathway, we treated the OVCAR3-M cells with SFN and the AKT agonist SC79. After adding SC79, glycolytic enzymes inhibited by SFN, including HK1, HK2, and GLUT1, showed a significant rebound (Figure S3). This suggests that SFN selectively suppresses key glycolytic enzymes in *PIK3CA*-mutated OC by inhibiting the PI3K/Akt signaling pathway, and that SC79 reverses the suppression of HK1, HK2, GLUT1, and p-AKT. This further suggests that SFN inhibits the expression of glycolysis-related enzymes by inhibiting the PI3K/Akt pathway and selectively reduces cancer cell proliferation in *PIK3CA* mutant cells.

3.6. SFN selectively inhibits the TCA cycle in *PIK3CA*-mutated cells

To further verify the effect of SFN on the TCA cycle, we used the Seahorse XF96 Analyzer to measure oxygen consumption rate in A2780, OVCAR3, OVCAR3-WT, and OVCAR3-M cells after 24 h of SFN treatment. Notably, SFN significantly inhibited the oxygen consumption rate in OC cells, leading to greater reductions in basal oxygen consumption, reserve

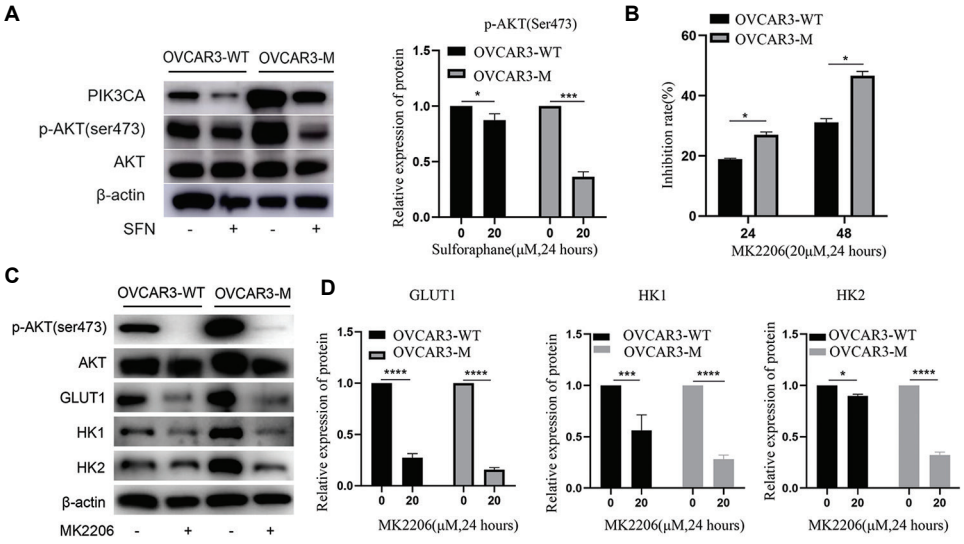

Figure 5. Sulforaphane (SFN) selectively inhibits glycolysis in *PIK3CA*-mutated cells via the phosphoinositide 3-kinase (PI3K)/protein kinase B (Akt)/hexokinase (HK) signaling pathway. (A) SFN inhibits AKT phosphorylation levels. (B) Inhibitory rate of ovarian cancer (OC) cells after treatment with 20 μM MK2206 for different durations. (C and D) Expression of proteins related to the PI3K/Akt and glycolysis pathways after treatment with 20 μM of MK2206 for different durations. Data from three independent experiments are shown as mean ± standard deviation. Statistical significance determined at *p<0.05; **p<0.01; ***p<0.001; and ****p<0.0001; ns indicates not significant. "+" indicates with; "−" indicates without.
Abbreviations: GLUT1: Glucose transporter 1; HK: Hexokinase.

respiratory capacity, and oxygen consumption associated with adenosine triphosphate production in *PIK3CA*-mutated cells compared with WT cells (Figure 6A). We further validated these results in the transfected cell lines, which confirmed the agreement with our initial findings (Figure 6B). These results indicated that SFN inhibited the TCA cycle in *PIK3CA*-mutated OC cells more significantly than in WT cells.

We further analyzed the levels of small-molecule metabolites of the TCA cycle in OVCAR3-WT and OVCAR3-M cells treated with SFN using untargeted metabolomics analysis. As shown in Figure 6C, following

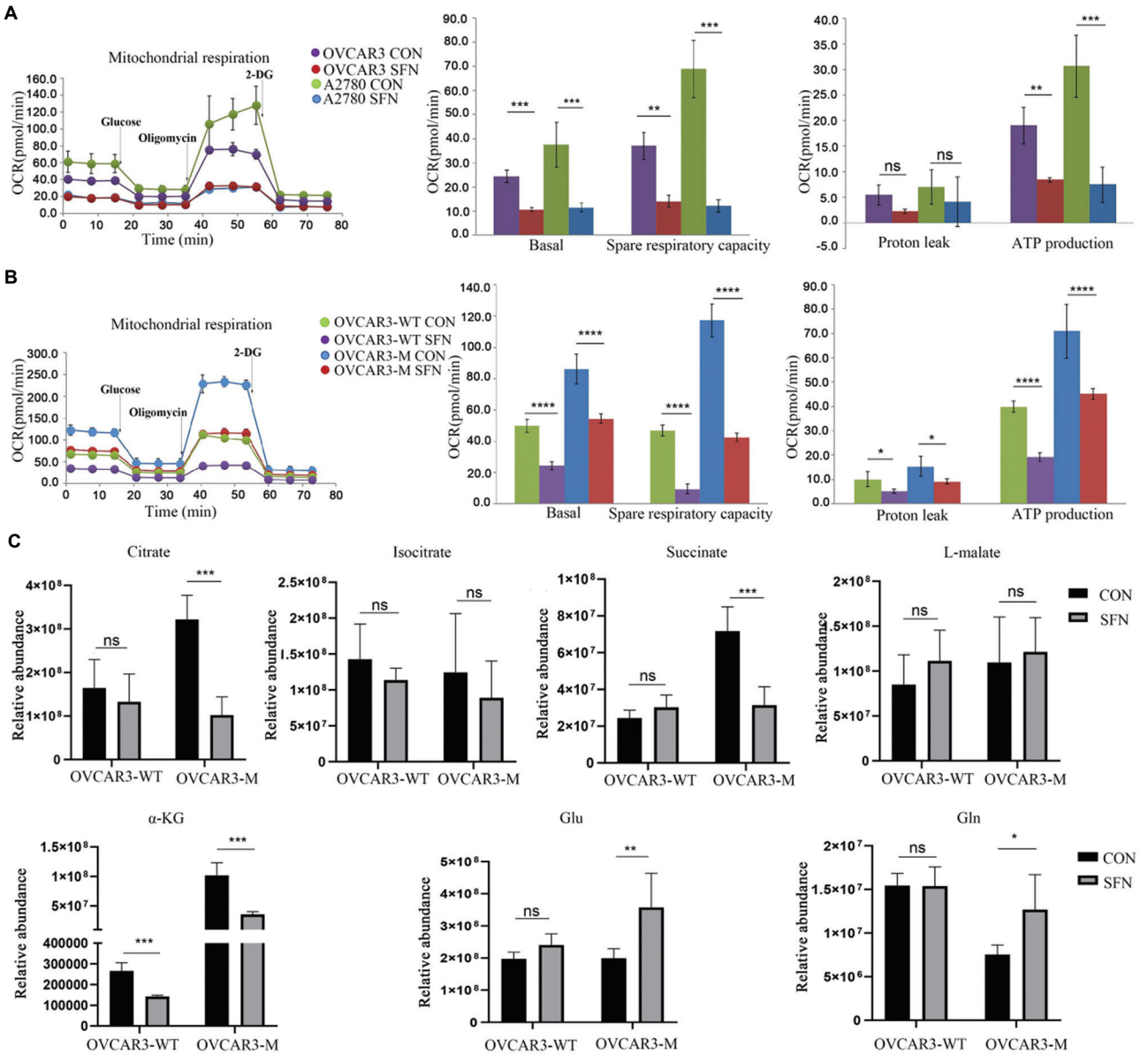

Figure 6. Sulforaphane (SFN) selectively inhibits the tricarboxylic acid (TCA) cycle activity in *PIK3CA*-mutated cells. (A & B) Mitochondrial stress test performed on A2780, OVCAR3, OVCAR3-WT (wild-type), and OVCAR3-M (mutant) cells. (C) The effect of SFN on small molecule metabolites in ovarian cancer (OC) cells. Data from three independent experiments are shown as mean ± standard deviation. Statistical significance determined at *p<0.05; **p<0.01; ***p<0.001; and ****p<0.0001; ns indicates not significant.

Abbreviations: α-KG: Alpha-ketoglutarate; ATP: Adenosine triphosphate; CON: Control; Gln: Glutaminase; Glu: Glutamine; OCR: Oxygen consumption rate.

SFN treatment, levels of α-KG, succinic acid, and citrate were reduced. Interestingly, after treatment with SFN, the levels of glutamine and glutamate increased in the mutant cells. This suggests that SFN may block the flow of α-KG generated by glutamine into the TCA cycle (Figure 6C). Previous experiments showed that SFN more strongly inhibits glycolysis in *PIK3CA*-mutated OC; therefore, we speculated that the more pronounced inhibition of SFN on the TCA cycle in these cells results from SFN concurrently inhibiting glycolysis and glutamine flux into the TCA cycle.

3.7. SFN selectively inhibits ovarian tumor growth in *PIK3CA*-mutated cells *in vivo*

To further study the antitumor effect of SFN, a mouse subcutaneous tumor model was established to compare the therapeutic response of *PIK3CA*-mutated and WT OC cells (Figure 7A). We divided the mice into the following four groups: OVCAR3-M + PBS, OVCAR3-WT + PBS, OVCAR3-M + SFN, and OVCAR3-WT + SFN. Compared to the OVCAR3-WT+PBS group, tumor volume and weight increased significantly in the OVCAR3-M+PBS group, as shown in the tumor appearance (Figure 7B). Dynamic observation of tumor growth (Figure 7C) revealed that the OVCAR3-M + PBS group had a significantly higher tumor growth rate than the OVCAR3-WT + PBS group, while SFN treatment strongly inhibited tumor growth in the OVCAR3-M group but weakly in the OVCAR3-WT group.

Further statistical analysis of tumor volume and weight (Figures 7D and E) showed that compared with the OVCAR3-WT + PBS group, the OVCAR3-M + PBS group had significantly increased tumor volume ($p<0.01$) and weight ($p<0.01$); after SFN treatment, the OVCAR3-M group exhibited significantly reduced tumor volume ($p<0.001$) and weight ($p<0.001$) compared to the same-genotype PBS group, with a stronger inhibitory effect than in the OVCAR3-WT group ($p<0.05$). These results indicate that SFN inhibits ovarian tumor growth, with a more prominent effect on *PIK3CA*-mutant tumors.

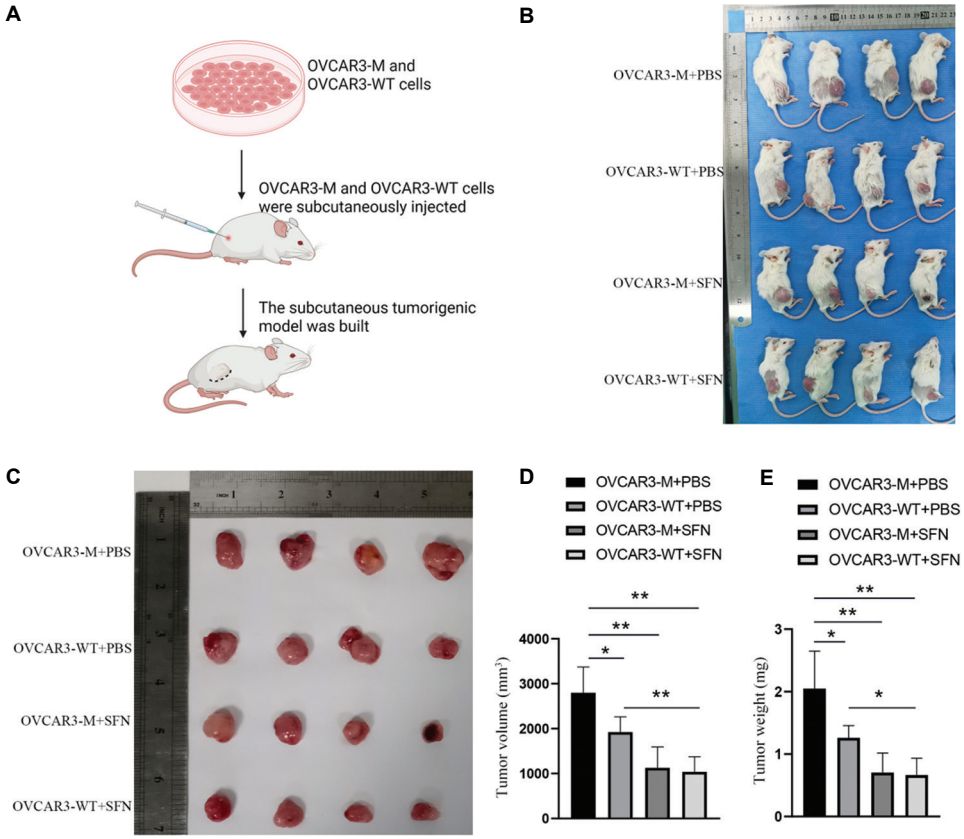

Figure 7. Sulforaphane (SFN) selectively inhibits ovarian tumor growth in *PIK3CA*-mutated cells *in vivo*. (A) Schematic diagram of subcutaneous tumor formation in mice. (B and C) Comparison of tumor size in mice between the OVCAR3-M (mutant) + phosphate-buffered saline (PBS) group, OVCAR3-WT (wild-type) + PBS group, OVCAR3-M+SFN group, and OVCAR3-WT+SFN group. (D and E) Comparison of tumor volume and weight in mice between the OVCAR3-M+PBS group, OVCAR3-WT+PBS group, OVCAR3-M+SFN group, and OVCAR3-WT+SFN group. Statistical significance determined at *$p<0.05$; **$p<0.01$; ***$p<0.001$; and ****$p<0.0001$; ns indicates not significant.

4. Discussion

Although treatment outcomes have improved in recent years, OC, which exhibits a relatively high incidence of *PIK3CA* mutations, remains the second leading cause of death among gynecological cancers.[29,30] Metabolic reprogramming, especially alterations in glucose metabolism, plays a crucial role in the survival of OC cells and contributes to the poor prognosis of OC.[31] Our study revealed that both glycolysis and the TCA cycle were concurrently upregulated in *PIK3CA*-mutated OC. Moreover, our study showed, for the first time, that SFN more effectively inhibited the enhanced glycolysis and TCA cycle activity in *PIK3CA*-mutated OC cells. This finding underscores the potential of SFN for the clinical treatment of OC, especially in patients with *PIK3CA* mutations.

PIK3CA mutations are prevalent in multiple cancers, especially breast, colorectal, ovarian, and brain cancers.[32-35] Furthermore, *PIK3CA* mutations are closely associated with patient prognosis across multiple cancer types. For example, in breast cancer, patients with *PIK3CA* mutations have higher mortality rates than those with WT *PIK3CA*, and patients who have died have presented metastases or recurrences.[36,37] In this study, we found that *PIK3CA* gene mutations accounted for 9.4% of OC and co-occurred with the *p53* gene in an analysis of 128 OC pathology specimens. Although *PIK3CA* mutations were not found to have a significant correlation with clinicopathological features, they were associated with poorer PFS, and may need to be further analyzed by expanding the sample size. Prior studies have shown that *PIK3CA* mutations promote glycolysis by increasing the mRNA and protein expression levels of key glycolytic enzymes, including LDHA/B, HK2, and GLUT1/4 in cervical cancer.[38] We found that *PIK3CA* mutations increased the expression of glycolytic enzymes, such as HK1, HK2, and PDK2, which aligns partially with previous findings. However, the direct relationship between *PIK3CA* mutations and the TCA cycle remains unknown. Our study is the first to identify a simultaneous increase in glycolysis and the TCA cycle in *PIK3CA*-mutated OC cells. Previous studies have shown that *PIK3CA* mutations can promote glycolysis by inducing the β-catenin/sirtuin three signaling pathway in cervical cancer.[38] We found that in *PIK3CA*-mutated OC cells, the PI3K/Akt/HK signaling pathway was activated, which promoted glycolysis and, subsequently, the TCA cycle. These factors are crucial for meeting the energy demands of rapidly proliferating cancer cells. The increased glycolytic and TCA cycle activity observed in *PIK3CA*-mutated cells further supports their aggressive growth profile compared to that of WT cells.

SFN has been shown to exert preventive and antitumor effects against various malignant tumors, including breast cancer, melanoma, and liver cancer.[39-42] In breast cancer, SFN can effectively inhibit the self-renewal and proliferation of cancer stem cells, thereby demonstrating strong potential for targeting cancer stem cells.[43] In this study, we discovered that SFN had a strong inhibitory effect on *PIK3CA*-mutated OC cell proliferation, which was achieved through the inhibition of glycolysis and the TCA cycle. Our *in vivo* experiments further confirmed that SFN inhibited OC growth, especially in tumors harboring *PIK3CA* mutations, thus revealing the role of SFN in the treatment of OC. Previous studies have shown that SFN suppresses high-glucose-induced pancreatic cancer progression through the nuclear factor erythroid 2-related factor 2 and adenosine monophosphate-activated protein kinase signaling pathways.[44] The current study showed that SFN selectively inhibited the PI3K/Akt/HK pathway, resulting in the selective inhibition of glycolysis in *PIK3CA*-mutated OC cells. In our study, *PIK3CA* wild-type OC cells grew significantly better than mutant cells in the presence of the AKT inhibitor MK2206, which indicates that cancer cells with *PIK3CA* mutations are selectively affected by the dependent regulation of activated AKT. This is consistent with the effect of SFN, which inhibits the proliferation of *PIK3CA*-mutated cells by inhibiting AKT activation. A critical consideration for the clinical translation of our findings is the pharmacological feasibility of achieving effective concentrations of SFN *in vivo*. Although SFN is derived from the diet and has limited oral bioavailability, studies have shown that plasma concentrations can reach low micromolar levels through the consumption of broccoli sprouts or standardized supplements, which is within the range that exerts biological effects in our *in vitro* models. Furthermore, ongoing research into novel delivery systems, such as nanoformulations, holds promise for further enhancing the bioavailability and therapeutic potential of SFN.

In addition to glycolysis, we discovered that SFN selectively inhibited the TCA cycle in *PIK3CA*-mutated OC cells. Mass spectrometry analysis showed that SFN reduced the levels of TCA-related intermediates, α-KG, succinic acid, and citrate, and this effect was more pronounced in *PIK3CA*-mutated OC cells. The TCA cycle is primarily fueled by intermediates derived from glycolysis; additionally, α-KG produced from glutamine metabolism can also contribute to the TCA cycle.[45] We found that SFN treatment increased glutamine levels in *PIK3CA*-mutated OC cells, suggesting that SFN inhibited the conversion of glutamine to α-KG. These findings suggest that the inhibition of the TCA cycle by SFN in *PIK3CA*-mutated OC may result from the dual inhibition of glycolysis and glutamine conversion to α-KG by SFN. This dual effect of SFN on glycolysis and the TCA cycle underscores its

potential as a therapeutic agent for targeting multiple metabolic vulnerabilities in *PIK3CA*-mutated cancers. Future investigations into the effects of SFN on glutamine metabolism in *PIK3CA*-mutated OC are warranted.

5. Conclusion

This study highlights the pivotal role of *PIK3CA* mutations in reconfiguring glycolysis and the TCA cycle. Glycolysis and the TCA cycle were found to be simultaneously enhanced in *PIK3CA*-mutated OC. Importantly, SFN selectively inhibited *PIK3CA*-mutated OC by targeting glycolysis and the TCA cycle through a PI3K/Akt-dependent mechanism. These results reveal the significant therapeutic effect of SFN on *PIK3CA*-mutated OC, thus providing a therapeutic option for future clinical trials for patients with OC.

Acknowledgments

The authors thank all patients and their families, as well as the contributors from the First Affiliated Hospital of Zhengzhou University who participated in this study.

Funding

This study was funded by the Natural Science Foundation of Henan (242300421273), the Beijing Science and Technology Innovation Medical Development Foundation (KC2021-JX-0186-130), the CSCO-Zai Ding Cancer Treatment Research Fund project (Y-zai2022/ms-0246), the National Outstanding Youth Science Fund Project of the National Natural Science Foundation of China, (81802770), and the Henan Provincial Health and Health Commission, Joint Co-construction Project of Medical Science and Technology Tackling Program in Henan Province (2018020056).

Conflict of interest

The authors declare no competing interests.

Author contributions

Conceptualization: Linlin Li
Formal analysis: Linlin Li, Ya Xie, Di Chen
Investigation: Zijiao Li, Yinli Su
Methodology: Linlin Li, Ya Xie, Di chen, Zijiao Li
Writing–original draft: Zijiao Li, Yinli Su
Writing–review & editing: Zijiao Li, Yinli Su, Han Wu, Liying Qin, Wan Fu, Xinyu Wang, Xuerou Wang, Longyang Li

Ethics approval and consent to participate

The study was approved by the Ethics Committee of the First Affiliated Hospital of Zhengzhou University (Approval no.: ChiECRCT20210071). All animal experiments were approved by the Animal Care Committee of the First Affiliated Hospital of Zhengzhou University (Approval no.: 2022-KY-0740-003). In addition, all experiments were conducted in accordance with relevant guidelines and regulations. Informed consent was obtained from all participants and/or their legal guardians.

Consent for publication

Participants have given their consent for data publication.

Availability of data

The datasets used and/or analyzed during the current study are available from the corresponding author upon reasonable request.

References

1. Bray F, Laversanne M, Sung H, *et al*. Global cancer statistics 2022: GLOBOCAN estimates of incidence and mortality worldwide for 36 cancers in 185 countries. *CA Cancer J Clin*. 2024;74:229-263.

   doi: 10.3322/caac.21834

2. Siegel RL, Giaquinto AN, Jemal A. Cancer statistics, 2024. *CA Cancer J Clin*. 2024;74:12-49.

   doi: 10.3322/caac.21820

3. Stine ZE, Schug ZT, Salvino JM, Dang CV. Targeting cancer metabolism in the era of precision oncology. *Nat Rev Drug Discov*. 2022;21:141-162.

   doi: 10.1038/s41573-021-00339-6

4. Warburg O. The metabolism of carcinoma cells. *J Cancer Res*. 1925;9:148-163.

   doi: 10.1158/jcr.1925.148

5. Elia I, Haigis MC. Metabolites and the tumour microenvironment: From cellular mechanisms to systemic metabolism. *Nat Metabol*. 2021;3:21-32.

   doi: 10.1038/s42255-020-00317-z.

6. Hegde S, Akbar H, Wellendorf AM, *et al.* Inhibition of RHOA activity preserves the survival and hemostasis function of long-term cold-stored platelets. *Blood*. 2024;144:1732-1746.

   doi: 10.1182/blood.2023021453

7. Xiao J, Wang S, Chen L, *et al*. 25-Hydroxycholesterol regulates lysosome AMP kinase activation and metabolic reprogramming to educate immunosuppressive macrophages. *Immunity*. 2024;57:1087-1104.e1087.

   doi: 10.1016/j.immuni.2024.03.021

8. Ladraa S, Zerbib L, Bayard C, *et al*. PIK3CA gain-of-function mutation in adipose tissue induces metabolic reprogramming with Warburg-like effect and severe endocrine disruption. *Sci Adv*. 2022;8:eade7823.

doi: 10.1126/sciadv.ade7823

9. Ikenoue T, *et al*. Functional analysis of *PIK3CA* gene mutations in human colorectal cancer. *Cancer Res*. 2005;65:4562-4567.

   doi: 10.1158/0008-5472.can-04-4114

10. Samuels Y, Wang Z, Bardelli A, *et al*. High frequency of mutations of the *PIK3CA* gene in human cancers. *Science*. 2004;304:554.

    doi: 10.1126/science.1096502

11. Turner NC, Im SA, Saura C, *et al.* Inavolisib-based therapy in PIK3CA-mutated advanced breast cancer. *New Engl J Med*. 2024;391:1584-1596.

    doi: 10.1056/nejmoa2404625

12. Wu Q, Ma J, Wei J, *et al.* FOXD1-AS1 regulates FOXD1 translation and promotes gastric cancer progression and chemoresistance by activating the PI3K/AKT/mTOR pathway. *Mol Oncol*. 2021;15:299-316.

    doi: 10.1002/1878-0261.12728

13. Xu JM, Wang Y, Wang YL, *et al*. PIK3CA mutations contribute to acquired cetuximab resistance in patients with metastatic colorectal cancer. *Clin Cancer Res*. 2017;23:4602-4616.

    doi: 10.1158/1078-0432.ccr-16-2738

14. Su WY, Tian LY, Guo LP, Huang LQ, Gao WY. PI3K signaling-regulated metabolic reprogramming: From mechanism to application. *Biochim Biophys Acta Rev Cancer*. 2023;1878:188952.

    doi: 10.1016/j.bbcan.2023.188952

15. Herms A, Colom B, Piedrafita G, *et al.* Organismal metabolism regulates the expansion of oncogenic PIK3CA mutant clones in normal esophagus. *Nat Genet*. 2024;56:2144-2157.

    doi: 10.1038/s41588-024-01891-8

16. Fusco N, Malapelle U, Fassan M, *et al.* PIK3CA mutations as a molecular target for hormone receptor-positive, HER2-negative metastatic breast cancer. *Front Oncol*. 2021;11:644737.

    doi: 10.3389/fonc.2021.644737

17. Vatte C, Al Amri AM, Cyrus C, *et al*. Helical and kinase domain mutations of PIK3CA, and their association with hormone receptor expression in breast cancer. *Oncol Lett*. 2019;18:2427-2433.

    doi: 10.3892/ol.2019.10565

18. Tan N, Wong M, Nannini MA, *et al.* Bcl-2/Bcl-xL inhibition increases the efficacy of MEK inhibition alone and in combination with PI3 kinase inhibition in lung and pancreatic tumor models. *Mol Cancer Ther*. 2013;12:853-864.

    doi: 10.1158/1535-7163.mct-12-0949

19. Mishra R, Patel H, Alanazi S, Kilroy MK, Garrett JT. PI3K inhibitors in cancer: Clinical implications and adverse effects. *Int J Mol Sci*. 2021;22:3464.

    doi: 10.3390/ijms22073464

20. Shi Z, Zeng H, Zhao B, *et al.* Sulforaphane reverses the enhanced NSCLC metastasis by regulating the miR-7-5p/c-Myc/LDHA axis in the acidic tumor microenvironment. *Phytomedicine*. 2024;133:155874.

    doi: 10.1016/j.phymed.2024.155874

21. Huang L, Wang J, Wang X, *et al*. Sulforaphane suppresses bladder cancer metastasis via blocking actin nucleation-mediated pseudopodia formation. *Cancer Lett*. 2024;601:217145.

    doi: 10.1016/j.canlet.2024.217145

22. Li L, Ma P, Nirasawa S, Liu H. Formation, immunomodulatory activities, and enhancement of glucosinolates and sulforaphane in broccoli sprouts: A review for maximizing the health benefits to human. *Crit Rev Food Sci Nutr*. 2024;64:7118-7148.

    doi: 10.1080/10408398.2023.2181311

23. Gong TT, Liu XD, Zhan ZP, Wu QJ. Sulforaphane enhances the cisplatin sensitivity through regulating DNA repair and accumulation of intracellular cisplatin in ovarian cancer cells. *Exp Cell Res*. 2020;393:112061.

    doi: 10.1016/j.yexcr.2020.112061

24. Justin S, Rutz J, Maxeiner S, *et al.* Chronic sulforaphane administration inhibits resistance to the mTOR-inhibitor everolimus in bladder cancer cells. *Int J Mol Sci*. 2020;21:4026.

25. Calcabrini C, Maffei F, Turrini E, Fimognari C. Sulforaphane potentiates anticancer effects of doxorubicin and cisplatin and mitigates their toxic effects. *Front Pharmacol*. 2020;11:567.

    doi: 10.3389/fphar.2020.00567

26. Kallifatidis G, Labsch S, Rausch V, *et al*. Sulforaphane increases drug-mediated cytotoxicity toward cancer stem-like cells of pancreas and prostate. *Mol Ther*. 2011;19:188-195.

    doi: 10.1038/mt.2010.216

27. Bose C, Awasthi S, Sharma R, *et al*. Sulforaphane potentiates anticancer effects of doxorubicin and attenuates its cardiotoxicity in a breast cancer model. *PLoS One*. 2018;13:e0193918.

    doi: 10.1371/journal.pone.0193918

28. Liu P, Zhang B, Li Y, Yuan Q. Potential mechanisms of cancer prevention and treatment by sulforaphane, a natural small molecule compound of plant-derived. *Mol Med*. 2024;30:94.

    doi: 10.1186/s10020-024-00842-7

29. Du Bois A, Reuss A, Pujade-Lauraine E, *et al*. Role of surgical outcome as prognostic factor in advanced epithelial

ovarian cancer: A combined exploratory analysis of 3 prospectively randomized phase 3 multicenter trials: By the arbeitsgemeinschaft gynaekologische onkologie studiengruppe ovarialkarzinom (AGO-OVAR) and the Groupe d'Investigateurs nationaux pour les etudes des cancers de l'Ovaire (GINECO). *Cancer*. 2009;115:1234-1244.

doi: 10.1002/cncr.24149

30. Shayesteh L, Lu Y, Kuo WL, *et al.* PIK3CA is implicated as an oncogene in ovarian cancer. *Nat Genet*. 1999;21:99-102.

doi: 10.1038/5042

31. Tan Y, Li J, Zhao G, *et al*. Metabolic reprogramming from glycolysis to fatty acid uptake and beta-oxidation in platinum-resistant cancer cells. *Nat Commun*. 2022;13:4554.

doi: 10.1038/s41467-022-32101-w

32. Li X, Mak VC, Zhou Y, *et al*. Deregulated Gab2 phosphorylation mediates aberrant AKT and STAT3 signaling upon PIK3R1 loss in ovarian cancer. *Nat Commun*. 2019;10:716.

doi: 10.1038/s41467-019-08574-7

33. Hortobagyi GN, Stemmer SM, Burris HA, *et al*. Updated results from MONALEESA-2, a phase III trial of first-line ribociclib plus letrozole versus placebo plus letrozole in hormone receptor-positive, HER2-negative advanced breast cancer. *Ann Oncol*. 2018;29:1541-1547.

doi: 10.1093/annonc/mdy155

34. Yaeger R, Chatila WK, Lipsyc MD, *et al.* Clinical sequencing defines the genomic landscape of metastatic colorectal cancer. *Cancer Cell*. 2018;33:125-136.e3.

doi: 10.1016/j.ccell.2017.12.004

35. McNicholas M, De Cola A, Bashardanesh Z, *et al.* A compendium of syngeneic, transplantable pediatric high-grade glioma models reveals subtype-specific therapeutic vulnerabilities. *Cancer Discov*. 2023;13:1592-1615.

doi: 10.1158/2159-8290.Cd-23-0004

36. Vasan N, Toska E, Scaltriti M. Overview of the relevance of PI3K pathway in HR-positive breast cancer. *Ann Oncol*. 2019;30:x3-x11.

doi: 10.1093/annonc/mdz281

37. Song KW, Edgar KA, Hanan EJ, *et al*. RTK-dependent inducible degradation of mutant PI3Kα drives GDC-0077 (Inavolisib) efficacy. *Cancer Discov*. 2022;12:204-219.

doi: 10.1158/2159-8290.Cd-21-0072

38. Jiang W, He T, Liu S, *et al.* The PIK3CA E542K and E545K mutations promote glycolysis and proliferation via induction of the β-catenin/SIRT3 signaling pathway in cervical cancer. *J Hematol Oncol*. 2018;11:139.

doi: 10.1186/s13045-018-0674-5

39. Pradeep Prabhu P, Mohanty B, Lobo CL, *et al.* Harnessing the nutriceutics in early-stage breast cancer: Mechanisms, combinational therapy, and drug delivery. *J Nanobiotechnol*. 2024;22:574.

doi: 10.1186/s12951-024-02815-8

40. Sundaram MK, Preetha R, Haque S, *et al.* Dietary isothiocyanates inhibit cancer progression by modulation of epigenome. *Semin Cancer Biol*. 2022;83:353-376.

doi: 10.1016/j.semcancer.2020.12.021

41. Joković N, Pešić S, Vitorović J, *et al.* Glucosinolates and their hydrolytic derivatives: Promising phytochemicals with anticancer potential. *Phytother Res PTR*. 2024;39:10.

doi: 10.1002/ptr.8419

42. Tomooka F, Kaji K, Nishimura N, *et al*. Sulforaphane potentiates gemcitabine-mediated anti-cancer effects against intrahepatic cholangiocarcinoma by inhibiting HDAC activity. *Cells*. 2023;12:687.

doi: 10.3390/cells12050687

43. Dandawate PR, Subramaniam D, Jensen RA, Anant S. Targeting cancer stem cells and signaling pathways by phytochemicals: Novel approach for breast cancer therapy. *Semin Cancer Biol*. 2016;40-41:192-208.

doi: 10.1016/j.semcancer.2016.09.001

44. Chen X, Jiang Z, Zhou C, *et al*. Activation of Nrf2 by sulforaphane inhibits high glucose-induced progression of pancreatic cancer via AMPK dependent signaling. *Cell Physiol Biochem*. 2018;50:1201-1215.

doi: 10.1159/000494547

45. Jo S, Seo M, Nguyen TH, *et al.* Biosynthesis-encoded lipogenic Acetyl-CoA measurement using NMR reveals glucose-driven lipogenesis and glutamine's alternative roles in kidney cancer. *J Am Chem Soc*. 2024;146:33753-33762.

doi: 10.1021/jacs.4c11809